arXiv:1504.02629v3 [cond-mat.mtrl-sci] 19 Apr 2016

Impact of lattice defects and electron correlations on the magnetic properties of Sr_2FeMoO_6

M. Hoffmann,[1, 2, *] V.N. Antonov,[3, 4] L.V. Bekenov,[3, 4] K. Kokko,[5, 6] W. Hergert,[2] and A. Ernst[4]

[1] *IFW Dresden, P.O. Box 270116, D-01171 Dresden, Germany*
[2] *Institute of Physics, Martin Luther University Halle-Wittenberg, Von-Seckendorff-Platz 1, 06120 Halle, Germany*
[3] *Institute for Metal Physics, 36 Vernadsky Street, 03142 Kiev, Ukraine*
[4] *Max Planck Institute of Microstructure Physics, Weinberg 2, 06120 Halle, Germany*
[5] *Department of Physics and Astronomy, University of Turku, FIN-20014 Turku, Finland*
[6] *Turku University Centre for Materials and Surfaces (MatSurf), Turku, Finland*

(Dated: April 20, 2016)

In this *ab initio* study, we focused on the influence of chemical composition and correlation effects on the electronic and magnetic properties of Sr_2FeMoO_6 (SFMO). We considered the appearance of the two most important lattice defects – oxygen vacancies and antisite defects. Different DFT-based methods were used, combining the advantages of a multiple scattering Green's function method, a spin-polarized fully relativistic linear-muffin-tin-orbital method, and the Vienna *ab initio* simulation package. Correlation effects were included with a self-interaction correction and a Hubbard U method. Using the magnetic force theorem, we determined the magnetic exchange coupling strength in SFMO with and without defects and determined the Curie temperatures T_C via Monte Carlo simulations. We found a ferrimagnetic ground state and verified its stability against electronic correlations or defects. The total magnetic moments decreased for both kinds of defects, either vacancies or antisite defects. This agreed well with the experimental observations. On the other hand, we could predict a strong variation of T_C as a function of the defect concentration. T_C could be increased by adding more oxygen vacancies while it could be reduced with increase of antisite disorder. The x-ray absorption spectra and x-ray magnetic circular dichroism at the Fe and Mo $L_{2,3}$, Fe K and Mo $M_{2,3}$ edges were simulated and compared with the available experimental results. The spectra agreed only after considering also oxygen vacancies. Thus, experimental observations of mixed valence states of the Fe ions in SFMO might be attributed to a certain amount of oxygen vacancies.

PACS numbers: 61.72.-y 75.30.Et 75.47.Lx 78.20.-e
Keywords: first-principles, HUTSEPOT, SFMO, oxide, critical temperature, defects, ASD, vacancies, XAS, XMCD

I. INTRODUCTION

Double perovskites $A_2BB'O_6$ (A = alkaline earth or rare earth and BB' are heterovalent transition metals such as B = Fe, Cr, Mn, Co, Ni; B' = Mo, Re, W) often demonstrate intrinsically complex magnetic structures and a wide variety of physical properties (see [1] for a review article on these materials).

Several experimental and theoretical studies have demonstrated that the double perovskite system Sr_2FeMoO_6 (SFMO) and other related materials exhibit a ferrimagnetic (FiM) half-metallic ground state with a high Curie temperature of 420 K [2]. The physical origin of the magnetoresistance in SFMO is half-metallicity [3], i.e., the material is an insulator in one of the spin channels, but a metal in the other. This leads to a complete spin polarization at the Fermi level, which immediately suggests their application as a source of spin polarized charge carriers in spintronic devices. Therein, SFMO will be used mainly as a thin film, and many attempts were made to grown high quality SFMO films [4–8]. But all these films yield a reduced Curie temperature, which is up to 80 K smaller than for bulk samples [7, 8], and even for bulk SFMO the theoretical magnetic moment of 4 μ_B was never experimentally observed. Such variations were attributed to lattice defects like grain boundaries or point defects. The latter includes swapping of Fe and Mo ions, antisite disorder (ASD), and oxygen vacancies (V_O). Several studies contributed to a theoretical understanding of these point defects and their effect on the magnetic properties [9–15] but only few of them addressed explicitly the magnetic exchange interactions and the Curie temperature, T_C [9, 10, 14]. Thus, we studied from *ab initio* the variation of the magnetic properties of SFMO with point defects deploying a Green's function (GF) method with the coherent potential approximation (CPA) in order to understand experimental differences in the magnetic moments and the Curie temperatures. We calculated magnetic coupling constants using the magnetic force theorem [16]. They are used in a second step to calculate the Curie temperature. The whole procedure provides usually correct magnetic properties of systems with itinerant and strongly localized electrons, if the crystalline structure is known and the applied density functional approximation describes adequately the electronic structure of the studied system [17–23].

Before including defects, we compared our numerical

---

[*] mart.hoffi@gmail.com

results of the electronic structure and magnetic properties of defect-free SFMO with previous theoretical [9–15] and experimental studies as a first validation step. Experiments on SFMO included numerous methods like photoemission spectroscopy (PES) [24–26], Mössbauer spectroscopy [27, 28], neutron scattering [29–31] or x-ray absorption spectroscopy (XAS) and x-ray magnetic circular dichroism (XMCD) measurements [32–35]. Since the XAS and XMCD spectroscopy is very sensitive to the electronic structure and the local environment, fitting calculated spectra to the available experimental results can provide important information about the chemical composition, the ionic valency and the degree of electronic correlations in the system. Thus, we simulated the XAS and XMCD spectra with our method and found a better agreement than previous density functional calculations [36]. Our results indicate as well a mixed valency of the Fe ion (Fe^{2+} or Fe^{3+}) observed by experiments [28, 29, 33, 34], but we can also follow from our study that the mixed valency might be mainly caused by oxygen vacancies.

In contrast to some previous theoretical studies [10, 24], we obtained half-metallic SFMO only if electron correlation effects were considered – in accordance with [11, 15, 37]. Within the adapted experimental lattice structure [38], the expected FiM state of SFMO was the stable magnetic ground state as long as the electronic structure showed half-metallicity. We traced the gradual transition from strong band magnetism in metallic SFMO to the ferrimagnetism in half-metallic SFMO and the corresponding critical temperatures by varying the electronic correlation parameter U_{eff}. Finally, we modeled point defects up to 15 % and 10 % for ASD and oxygen vacancies. The calculated magnetic moments and T_{C} showed significant variations in good agreement with available comparable studies but were also strongly depending on the correct description of the underlying electronic structure.

In the following section, we describe the lattice structure of SFMO used in our calculations. Details about the calculation techniques are given in the next section. The influence of the electronic correlations and the lattice defects on the electronic structure is discussed in Sec. IV. Their effect on the magnetic properties, such as the magnetic moment or the Curie temperature, is shown in Sec. V. We present in the Sec. VI the XAS and XMCD calculations for the SFMO compound and compare them with previously measured spectra. The results are summarized in the last section.

II. LATTICE STRUCTURE

For our calculations of SFMO, we adopted the experimentally found double perovskite structure, where the oxygen atoms provide an octahedral environment around the Fe and Mo sites. The FeO_6 and MoO_6 octahedra alternate along the three cubic axes, while the Sr atoms occupy the hollow site formed by the corners of the FeO_6 and MoO_6 octahedra at the body-centered positions (see Fig. 1).

TABLE I. Variation of the experimental lattice constants and oxygen positions of SFMO from several references. Fe occupies consistently (0, 0, 0). The Wyckoff positions of the oxygen atoms are $(0, 0, z)$ and $(x, y, 0)$. The positions of the other atoms are described in the text.

a (Å)	c (Å)	$c/a/\sqrt{2}$	x	y	z	Ref.
5.5729	7.9077	1.003353	0.248	$= x$	0.235	[40, 44]
5.573	7.902	1.002612	0.2464	$= x$	$= x$	[38]
5.5752	7.89251	1.001009	0.2610	0.2333	0.2474	[41]
5.587	7.894	0.999087	0.248	$= x$	0.235	[45]

SFMO was found to be cubic ($Fm\bar{3}m$) in the paramagnetic phase, but changes into a tetragonal-type structure below a critical temperature [31, 39]. A representative choice of experimentally observed lattice constants is collected in Tab. I. Their variation between the smallest and largest value is quite small (0.25 % and 0.17 % for a and c, respectively) and the cubic symmetry would be represented by a c/a ratio of $\sqrt{2}$. Thus, we see from the data in Tab. I that the deviation from the cubic symmetry is small as well.

In general, the Sr atoms occupy the 4d Wyckoff positions $(0, 1/2, 1/4)$. Depending on the publication, the Fe atoms occupy the 2a Wyckoff pos. $(0, 0, 0)$ and Mo the 4d Wyckoff pos. $(0, 0, 1/2)$, or vice versa. The positions of the oxygen atoms is not definite and varies between different studies (see Tab. I). They sit either exactly between Mo and Fe, which gives the body centered tetragonal structure type ($I4/mmm$; No. 139 [38, 40]) or the oxygen octahedra are slightly distorted ($I4/m$, No. 87 [41, 42]). In any case, there are two types of oxygen atoms with O_z at the 4e Wyckoff pos. $(0, 0, z)$ and O_{xy} at the 8h Wyckoff pos. $(x, y, 0)$ while the Fe atom position is $(0, 0, 0)$ (see Fig. 1).

Since the changes of the lattice constants are small, we used for simplicity the more symmetric body centered tetragonal structure type and the lattice constant from [38] as input for our study. As long it is not stated otherwise, we used the primitive unit cell with one functional unit of SFMO (see blue arrows in Fig. 1).

III. COMPUTATIONAL DETAILS

For the microscopic understanding of the SFMO compound, we combined the theoretical results of three computational methods, namely the multiple scattering Green's function method HUTSEPOT [46], the spin-polarized fully relativistic linear-muffin-tin-orbital (SPR-LMTO) method [47–49] and the Vienna *ab initio* simulation package (VASP) [50, 51]. The main investigation of the electronic and magnetic properties were conducted with HUTSEPOT, whereas the XAS and XMCD spectra were calculated within the SPR-LMTO, and necessary

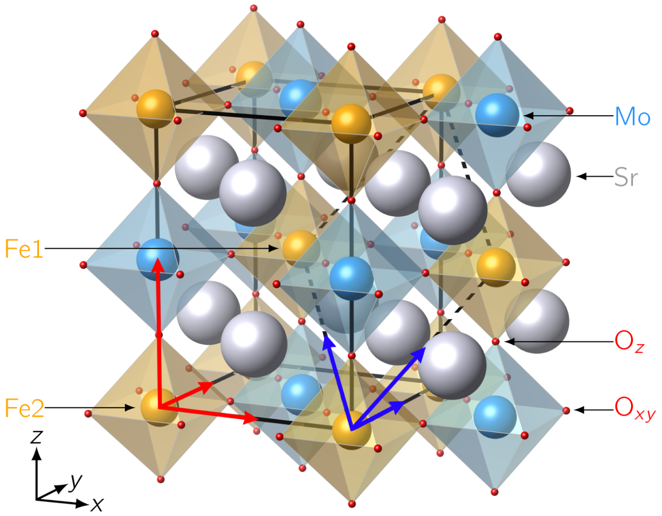

FIG. 1. (Color online) The double perovskite structure of SFMO. The colored polyhedra visualize the octahedral surroundings of the Fe and Mo atoms (orange and blue) [43]. Following from the tetragonal symmetry, two different oxygen positions appear (marked with O_{xy} and O_z). The tetragonal supercell is shown by the black solid lines and the red arrows. It contains two functional units with two Fe sites (Fe1, Fe2). The black dashed lines and the blue arrows indicate the primitive unit cell.

structure relaxations were achieved with VASP.

a. Electronic structure The orbital resolved density of states (DOS) were calculated with HUTSEPOT within the full-charge density approximation to the crystal potential. For the Green's function, the angular momentum cutoff was $l_{\max} = 3$ and the Brillouin zone integration was done with a $\boldsymbol{k}$-point mesh of $12\times12\times12$. The complex energy contour was integrated over 24 Gaussian quadrature points. With the Green's function $G(E)$ of the system, all quantities of interest like the local density of states (LDOS) follow in a straightforward way.

The exchange-correlation functional of a GGA-type was used very successful in the context of SFMO [3, 52]. Within the Green's function method, we used in particular the version of Perdew, Burke and Ernzerhof (PBE) [53, 54]. In order to deal with the strong correlations in the oxide system, the self-interaction correction (SIC) [46] and the GGA+U approach of Dudarev *et al.* [55] implemented in the Green's function method were used ($U_{\mathrm{eff}} = U - J$). For the SIC, only the LDA exchange-correlation functional can be used.

We note, that the calculation of the electronic structure in SFMO is very sensitive to the choice of the atomic radii and the crystalline structure. We used the atomic radii, obtained from the largest overlap of atomic potentials. Using smaller radii for the Fe atoms led to a half-metallic solution independent of the exchange-correlation functional – either LDA or GGA. We observed the same also within the SPR-LMTO method.

b. Magnetic properties We calculated the interatomic exchange coupling parameters J_{ij} from *ab initio* using the magnetic force theorem [16] implemented within HUTSEPOT. The underlying magnetic reference state for these calculations was the FiM solution – Fe moments align parallel to each other and Mo moments align antiparallel to the Fe moments. This was also identified as stable magnetic ground state by the calculation of the corresponding magnon spectrum. On the other hand, the magnetic moments of Mo are often considered as induced moments. Such moments will vanish above the T_{C} and alter, thereby, the numerical results for T_{C}. We can model a paramagnetic (PM) state at high temperature via the disordered local moment (DLM) theory [56, 57] and the corresponding results will be compared with the conventional calculations. Often, this procedure allows a better estimation of T_{C} [23].

In any case, the J_{ij} can be used in a Monte Carlo (MC) simulation to obtain the critical temperatures (details in [18, 58, 59]). Therefore, the unit cell in Fig. 1 was repeated $20 \times 20 \times 20$ times to form a large cluster. We considered also periodic boundary conditions and restricted the calculation only to the magnetic atoms of the unit cell. The starting point was a high-temperature disordered state above the critical temperature T_{C}. In the course of the simulations, the temperature was stepwise reduced until magnetic ordering was reached. For each temperature T, the thermal equilibrium was assumed to be reached after 20 000 MC steps. The thermal averages were determined over 20 000 additional MC steps. T_{C} was then obtained from the temperature dependency of the magnetic susceptibility and the heat capacity within a numerical uncertainty range of $\pm 5\,\mathrm{K}$. For comparison, T_{C} was also calculated with the mean-field approximation (MFA) and random-phase approximation (RPA) [60].

c. Simulation of x-ray spectra The x-ray absorption and dichroism spectra were calculated with the SPR-LMTO method taking into account the exchange splitting of the core levels. The approach for the XAS and XMCD simulations is described in our previous papers [61]. The finite lifetime of a core hole was accounted for by folding the spectra with a Lorentzian. The widths of core level spectra $\Gamma_{\mathrm{L}_2} = 1.14\,\mathrm{eV}$ and $\Gamma_{\mathrm{L}_3} = 0.41\,\mathrm{eV}$ for Fe, $\Gamma_{\mathrm{L}_2} = 1.83\,\mathrm{eV}$, $\Gamma_{\mathrm{L}_3} = 1.69\,\mathrm{eV}$ and $\Gamma_{\mathrm{M}_{2,3}} = 2.1\,\mathrm{eV}$ for Mo were taken from [62]. The finite apparative resolution of the spectrometer was accounted for by a Gaussian of width 0.6 eV.

In our SPR-LMTO simulations, the basis set consisted of the s, p, and d LMTO's for the Sr, Fe, Mo and O sites. The $\boldsymbol{k}$-space integrations were performed with the improved tetrahedron method [63] and the self-consistent charge density was obtained with 1063 irreducible $\boldsymbol{k}$-points. We used a relativistic generalization of the LDA+U method, which takes into account the spin-orbit coupling so that the occupation matrix of localized electrons becomes non-diagonal in spin indexes. This method is described in detail in our previous paper [64] including the procedure to calculate the screened Coulomb U and exchange J integrals, as well as the Slater integrals F^2, F^4, and F^6. The constrained LSDA calculations produce $J = 0.85\,\text{eV}$ for the Fe site in SFMO. In order to be consistent with the other methods, the Hubbard U has been used as an external parameter.

d. Defects We investigated the influence of two types of point defects in $\text{Sr}_2[\text{Fe}_{1-x}\text{Mo}_x][\text{Mo}_{1-x}\text{Fe}_x]\text{O}_{6-\delta}$, namely, oxygen-deficiency δ and the ASD x. The latter means a swap of an Fe ion with a Mo ion and vice versa keeping the stoichiometry of SFMO constant.

Both were simulated with the coherent potential approximation in the GF method, while the lattice structure has to be kept static. Although some experimental studies report no random distribution but segregation into small clusters and formation of antiphase boundaries [65], the ASD was modeled by interchanging randomly Fe and Mo. At the low concentration limit, the CPA is appropriate to reproduce the electronic structure of both randomly distributed and clustered disorder. Advanced schemes [66], which go beyond the single-site approximation of the CPA need still high computational resources for larger unit cells and are beyond the scope of this investigation. For the oxygen vacancies, a certain percentage of empty spheres was introduced at the lattice sites of the oxygen ions. The typical oxygen-deficiency δ ranges between 0.006 to 0.36 [67–69]. This represents 0.1 at. % to 6 at. % of the total oxygen amount in defect-free SFMO.

In addition, we used a supercell approximation with a cell of two functional units of SFMO (see red arrows in Fig. 1). This supercell was relaxed with VASP including either ASD or a single oxygen vacancy close to Fe2. For the antisite defects, we found, similarly as in [11], no significant relaxation. The relaxation with VASP for a single oxygen vacancy led to a distance of 1.9722 Å between Fe2 and the vacancy – an increase by 1.5 %. The correspondent distance between the Fe1 ion and the oxygen vacancy was reduced by 0.5 % to 4.4054 Å.

IV. ELECTRONIC STRUCTURE

Although the half-metallic solution was previously obtained within the LDA and the GGA with different calculation techniques [3, 70], the Green's function method yielded a metallic solution similar as in [11, 15, 37] with a nonzero density of states in both spin channels at the Fermi energy, E_F, independent of the use of LSDA or GGA (see Figs. S2 and S3 [71]). We also crosschecked the calculation of the DOS with the other methods and found similar results.

From this metallic state, a band gap in the majority spin channel emerges when correlation corrections are applied (either GGA+U [11, 37] or SIC [72]), and a half-metallic state forms [71]. Optical measurements determined a band gap of 0.5 eV, which should appear between the Mo $t_{2g}^{\uparrow}$ states and the Fe $e_g^{\uparrow}$ states [73]. This gap is rather small considering the position of the Fe $e_g^{\uparrow}$ states ($\approx 1.3\,\text{eV}$) measured by photoemission spectroscopy (PES) [24–26]. It might be that intermediate energy levels were introduced by defects, and allow additional optical transitions. Hence, we expected the Fe $e_g^{\uparrow}$ [74] states roughly at 1.3 eV below E_F. Applying the SIC in our calculations, the localization of the Fe d states was strongly overestimated and the states were too far below E_F, although the half-metallic ground state is well represented within the SIC [72]. In order to obtain a better agreement for the Fe $e_g^{\uparrow}$ state with the experimental observations, we calculated the DOS for several correlation parameters U_eff^Fe applied only to Fe d states [71], and found a good agreement for $U_\text{eff}^\text{Fe} = 2\,\text{eV}$ (see dashed line in Fig. 2). The main changes occur for the Fe $e_g^{\uparrow}$ states at E_F, which crossed E_F for $U_\text{eff}^\text{Fe} \gtrapprox 1\,\text{eV}$ and the band gap

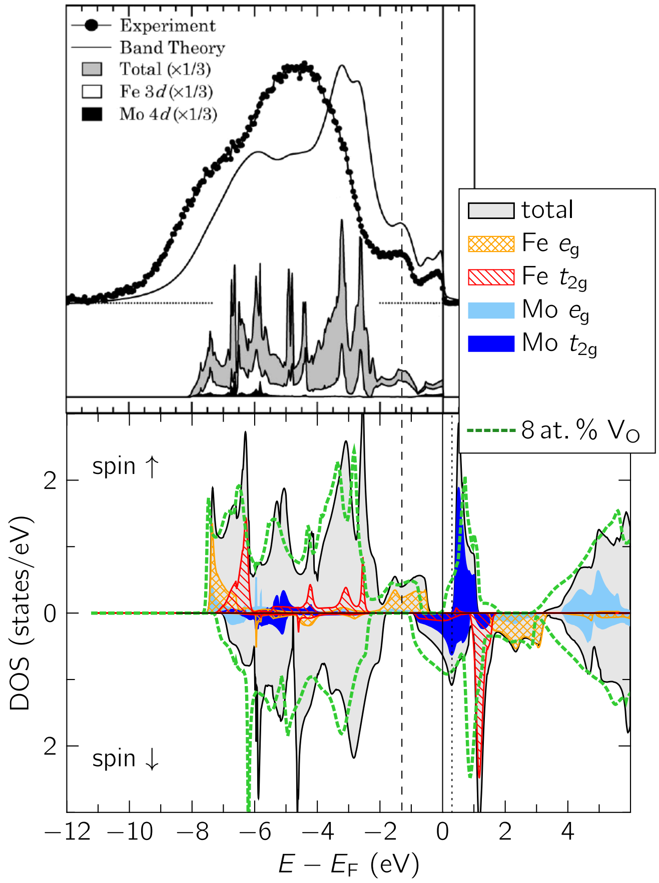

FIG. 2. (Color online) The upper panel shows the experimental and simulated PES of SFMO taken as a copy of Fig. 5(a) of Ref. [24] (some labels were removed). The lower panel represents the DOS for SFMO calculated with the GF method and $U_\text{eff}^\text{Fe} = 2\,\text{eV}$. The gray area shows the total DOS for defect-free SFMO. The colored regions indicate the LDOS for the d states of Fe (reddish) and Mo (bluish). The green dotted DOS includes 8 at. % of randomly distributed oxygen vacancies. Both plots are scaled with respect to the same energy scale and the Fermi energy at zero (black vertical line). The dashed line indicates the position of the Fe $e_g^{\uparrow}$ in the experimental PES.

emerged [71]. Then, almost all $d^{\uparrow}$ ($d^{\downarrow}$) states of Fe are occupied (unoccupied), which is represented by a formal Fe^{3+} valence state. For the Mo ions, almost all states are unoccupied, except the delocalized $t_{2g}^{\downarrow}$ states, which could be considered as a Mo^{5+} state. This situation was found in all self-consistent solutions with GGA+U and represents the generally accepted ground state of SFMO [3, 11, 14, 72]. Thus, we use it as well in the description of the magnetic properties below.

Although the finding of an appropriate value for $U_{\mathrm{eff}}^{\mathrm{Fe}}$, which was described above, is a rather standard procedure when dealing with strongly correlated systems, several aspects might influence the comparison between theoretical DOS and experimental PES data. Here, we emphasize two aspects. On the one hand, the calculated Fe $e_{g}^{\uparrow}$ states had a bandwidth of roughly 1 eV (see Fig. 2), whereby the PES measurement can not define the exact position of the Fe $e_{g}^{\uparrow}$ states. On the other hand, the conclusion about the contribution of the states to the PES is based on numerical calculations of defect-free SFMO [24]. Saitoh *et al.* [24] noticed possible ASD in their samples (up to 10 at. %) but could not account for defects in their theoretical interpretation. When we include within the CPA some atomic percent of ASD inside SFMO, the DOS is strongly varied as observed by many other studies [10–12, 15]. In particular, some states of the majority spin channel appear also at E_{F} and reduce the spin polarization, which is also observed experimentally [75]. In contrast, a low concentration of oxygen vacancies does not alter the half-metallic character of SFMO [11, 12, 76], but additional Fe $d^{\downarrow}$ and Mo $d^{\downarrow}$ states become occupied [11]. This indicates a lower valency of the Fe and Mo ions. Electrons of the removed oxygen atoms occupy states of Fe and Mo ions. A similar qualitative behavior was observed within our calculations of oxygen-deficient SFMO with CPA (green dashed line in Fig. 2). The intensity of the states in the spin down channel right below the Fermi energy is increased as obtained in Ref. [11], and the Fe $e_{g}^{\uparrow}$ states are shifted to lower energies. In addition, the averaging within the CPA broadens all states (see Fig. 2).

Taken as a whole, a direct comparison between the DOS and the PES data is complicated when considering all the various influences of electron correlations or possible defects. In order to have a point of reference for later discussions, we believe that $U_{\mathrm{eff}}^{\mathrm{Fe}} = 2\,\mathrm{eV}$ is a suitable compromise considering all available data. It is applied in the following, if not stated otherwise.

V. MAGNETIC PROPERTIES

The observed transition from a metallic to a half-metallic state influences as well the magnetic properties. We investigated theoretically the magnetic moments, the magnetic exchange coupling, and the Curie temperature of SFMO in dependence on the electron correlations and defect concentrations. All three numerical methods mentioned above showed a good qualitative agreement despite of the different exchange functionals. The ferrimagnetic ground state was always energetically favorable when comparing possible magnetic configurations and we did not observe a hint to spin spiral ordering as reported earlier [10]. In order to verify the magnetic ground state, we calculated the magnon spectrum for half-metallic SFMO (see Fig. 3). The spectrum shows two well separated modes. In accordance with our analysis of the corresponding site-resolved magnonic Green function, the positive mode is mainly associated with the collective precession of Fe magnetic moments, while the negative mode reflects the properties of Mo magnetic moments. The different signs of the modes indicate on a ferrimagnetic ground state, which is confirmed by our total energy calculations. The different observations might follow from our choice of taking the experimental lattice structure of SFMO instead of the undisturbed cubic lattice structure [10]. However, Solovyev [10] found that the FiM ground might be stabilized including breathing distortions of the oxygen octahedra. If the oxygen ion came closer to the Fe ions, the proposed spin spiral ordering became less favorable with respect to the FiM state but the half-metallicity was gone. These observations match ours. Our calculations within the GGA yielded for the experimental structure (where $d_{\text{Fe-O}}/d_{\text{Fe-Mo}} < 0.5$, see Tab. I) a metallic ground state as well.

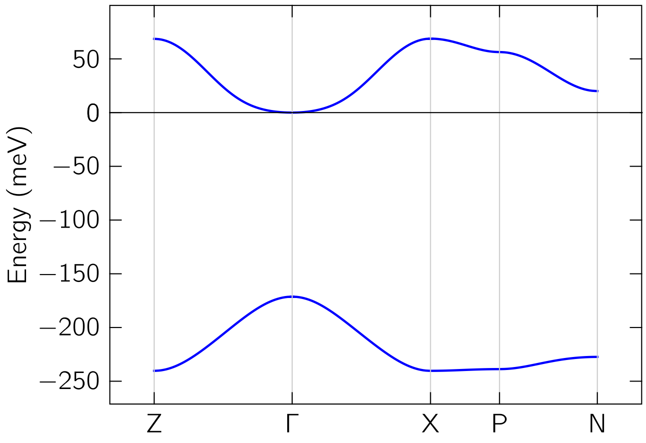

FIG. 3. Magnon spectrum of half-metallic SFMO ($U_{\mathrm{eff}}^{\mathrm{Fe}} = 2\,\mathrm{eV}$). Two well separated modes can be identified. One of them (positive) is associated mainly with the Fe magnetic atoms, while the other one (negative) with the Mo moments.

A. Magnetic moments

We calculated the spin and orbital moments in the FiM ground state. The Fe spin and orbital moments are parallel, whereas the spin and orbital Mo moments are antiparallel to each other, in accordance with Hund's third rule (see Tab. II). Our calculations for the metallic solution (weak electron correlation regime) provide for Fe a lower spin magnetic moment than in earlier calculations ($3.72\,\mu_\mathrm{B}$ to $3.97\,\mu_\mathrm{B}$ [3, 36, 77–79]). As soon as we observe half-metallic SFMO ($U_\mathrm{eff}^\mathrm{Fe} > 1\,\mathrm{eV}$), the Fe spin moment of $\approx 4\,\mu_\mathrm{B}$ is in a good agreement with the experimental neutron diffraction measurements [30] and the theoretical ideal value for the $\mathrm{Fe}^{3+}/\mathrm{Mo}^{5+}$ or $\mathrm{Fe}^{2+}/\mathrm{Mo}^{6+}$ valency configuration (see Tab. II). It remains quite stable and insensitive to the strength of the electron correlations. The orbital Fe magnetic moment of $0.041\,\mu_\mathrm{B}$ is very close to the FPLMTO result of Jeng and Guo [79] ($0.043\,\mu_\mathrm{B}$) and the LMTO results of Kanchana *et al.* [36] ($0.042\,\mu_\mathrm{B}$). The calculated spin and orbital moments of the Mo atom are always larger in comparison with earlier calculations [3, 36, 77–79].

We note that the spin and orbital magnetic moments were obtained from the XMCD experiments by using the sum rules, which relate the integrated signals over the spin-orbit split core edges of the circular dichroism to the ground state orbital and spin magnetic moments [80]. It is well known that the application of the sum rules sometimes results in an error up to 50 % [81]. To investigate the possible error of the sum rules in the case of SFMO we compare the spin and orbital moments obtained from the theoretically calculated XAS and XMCD spectra through sum rules with directly calculated LDA+U values. The number of the transition metal $3d$ electrons is calculated by integrating the occupied d local density of states inside the corresponding atomic spheres, which gives the values $n_d^\mathrm{Fe} = 6.737$ and $n_d^\mathrm{Mo} = 4.552$. The sum rules reproduce the spin magnetic moments within 4 % and 8 % and the orbital moments within 21 % and 14 % for Fe and Mo, respectively (see Tab. II).

The lower reported spin moments of the XMCD experiments compared to the theoretical value for Fe^{3+} ($4\,\mu_\mathrm{B}$) were always attributed to antisite disorder [9, 33, 67, 82]. We used again the CPA to investigate randomly distributed defects. The introduced Fe ions at the Mo sites (Fe_Mo) coupled strongly antiferromagnetically to the intrinsic Fe ions (see Fig. 7). Indeed, the total magnetic moment of SFMO is linearly reduced for ASD up to 15 at. %, independent of the strength of the electron correlations (see Fig. 4(a)). The slope of this reduction is in good agreement with the estimations by previous Monte Carlo simulations [9] and experiments [82].

TABLE II. The calculated spin m_s and orbital m_o magnetic moments (in μ_B) of Fe and Mo in defect-free SFMO compared with the measured magnetic moments. The moments m_s and m_o were obtained with the SPR-LMTO (1). In addition, we show m_s determined with the GF method (2). The sum rules are applied for the theoretically calculated XMCD spectra in the LDA+U approximation (SPR-LMTO). Experimental uncertainties are given in brackets behind the values.

	Fe		Mo	
method	m_s	m_o	m_s	m_o
LSDA$^{(1)}$	3.503	0.046	−0.456	0.034
LDA+$U^{(1)}$	4.104	0.041	−0.504	0.047
Sum rules$^{(1)}$	4.283	0.052	−0.464	0.041
GGA$^{(2)}$	3.090		−0.555	
GGA+$U^{(2)}$	3.921		−0.525	
Ref. [33][a]	3.05(20)	0.02(2)	−0.32(5)	−0.05(5)
Ref. [35][a]	2.80(30)	0.093(10)	−0.36(3)	−0.037(15)
Ref. [30][b]	4.1(1)		0.0(1)	
Ref. [36][c]	3.72	0.042	−0.29	0.020
Ref. [77][c]	3.97		−0.39	

[a] XMCD measurement
[b] Neutron diffraction experiment
[c] Theory

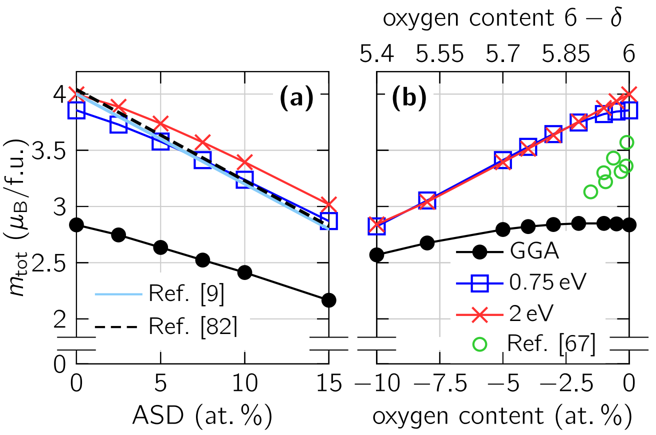

FIG. 4. Total magnetic moment m_tot in dependence on (a) the ASD, or (b) oxygen deficiency δ obtained with the GF method for metallic, nearly half-metallic and half-metallic SFMO (GGA, $U_\mathrm{eff}^\mathrm{Fe} = 0.75\,\mathrm{eV}$, and $U_\mathrm{eff}^\mathrm{Fe} = 2\,\mathrm{eV}$, respectively). Results of previous references are included.

On the other hand, oxygen vacancies reduce also the total magnetic moment [67], which agrees well with our theoretical results within the CPA. The reduction is purely linear for half-metallic SFMO ($U_\mathrm{eff}^\mathrm{Fe} = 2\,\mathrm{eV}$) (see Fig. 4(b)). The offset for $\delta = 0$ can be attributed to ASD of roughly 5 at. % to 8 at. % [67]. We want to emphasize the change of the slope for $U_\mathrm{eff}^\mathrm{Fe} = 0.75\,\mathrm{eV}$, where we observe the same slope as that of $U_\mathrm{eff}^\mathrm{Fe} = 2\,\mathrm{eV}$ only after adding few atomic percent of oxygen vacancies. As observed for the DOS, the randomly distributed oxygen vacancies have a similar effect as the correlation parameter $U_\mathrm{eff}^\mathrm{Fe}$. Both reduce the electron hopping between the Fe and Mo orbitals, and considering the oxygen vacancies results in half-metallic SFMO with the correct magnetic moment (compare blue and red lines in Fig. 4(b)).

B. Magnetic exchange interactions and Curie temperatures

In contrast to the magnetic moment, the calculated magnetic exchange parameters between the magnetic atoms and the critical temperatures are more sensitive to changes in the DOS. The most prominent coupling constants of the order of several meV have only a very

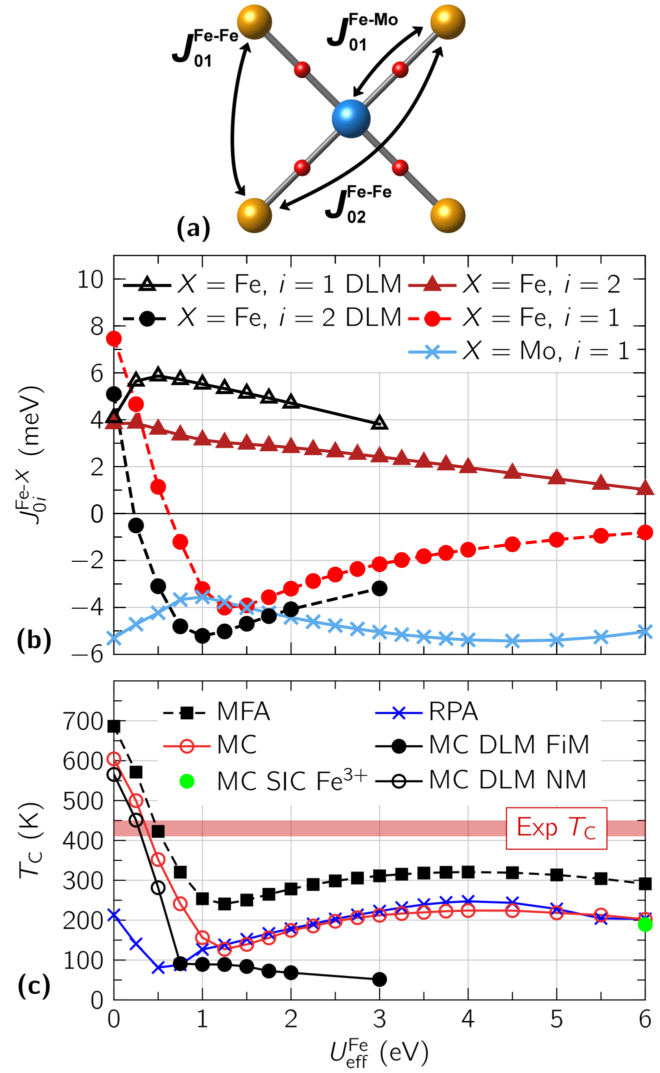

FIG. 5. (a) Sketch of the orientation of the important magnetic exchange interactions $J_{0i}^{\text{Fe-}X}$ between Fe and Mo ions (i is the shell index, X = Fe or Mo) [43]. (b) The $J_{0i}^{\text{Fe-}X}$ in the FiM or PM (DLM) reference state in dependence on $U_{\text{eff}}^{\text{Fe}}$. (c) Curie temperatures calculated with MFA, RPA, or MC method. They are compared with the experimental T_C range. The observed ground state change in the DLM model is marked with open and full circles (see text). The result of the calculation with SIC is shown for comparison.

restricted range up to 7.9 Å. This includes only the interactions up to the next nearest neighbor Fe ions $J_{02}^{\text{Fe-Fe}}$ (sketched in Fig. 5(a)). As it is discussed below, only these magnetic couplings dominate the magnetic behavior with respect to the electron correlations. The more distant exchange constants (up to 12.49 Å) were one order of magnitude smaller and became even more reduced with increasing $U_{\text{eff}}^{\text{Fe}}$. All the others could be considered to be zero. Due to the tetragonal structure, all magnetic exchange interactions show a small asymmetry with respect to those with a component in z direction. For clarity, only the coupling constants in the x-y-plane are shown.

We considered two different calculation schemes:

(i) On the one hand side, the calculations of J_{ij} were performed in the FiM reference state (red and blue in Fig. 5(b)). We observe a strong antiferromagnetic (AFM) coupling between Fe and Mo ions. Its absolute size becomes reduced around $U_{\text{eff}}^{\text{Fe}} \approx 1\,\text{eV}$ and increases again afterwards. The nearest neighbor Fe–Fe coupling constants, $J_{01}^{\text{Fe-Fe}}$, decrease linearly from 4 meV to 1 meV with increasing $U_{\text{eff}}^{\text{Fe}}$. It might be correlated to the linear changes in the Fe $e_g^{\uparrow}$ states. This behavior is typical for the application of U_{eff}. The stronger localization of the orbitals leads to a decrease of the electron hopping and, thereby, to a decrease in the magnetic coupling strength. Nevertheless, the behavior of the next nearest Fe–Fe coupling constants, $J_{02}^{\text{Fe-Fe}}$, is more complicated (see Fig. 5(b)). These show a strong linear reduction until the coupling switches to a negative value (AFM). At $U_{\text{eff}}^{\text{Fe}} \approx 1\,\text{eV}$, the slope is reversed but the $J_{02}^{\text{Fe-Fe}}$ coupling constants remain negative. Only the absolute values decrease.

These results deviate from the former calculations of magnetic exchange interactions of Solovyev [10]. He found for purely cubic SFMO no metallic DOS and, hence, no positive $J_{02}^{\text{Fe-Fe}}$ but a rather strong AFM coupling of −21.5 eV. The observations might qualitatively match our results for half-metallic SFMO – positive $J_{01}^{\text{Fe-Fe}}$ and negative $J_{02}^{\text{Fe-Fe}}$ – but together with a small Fe–Mo coupling of −1.21 eV, the FiM state is not stable according to his criterion of instability [10]

$$2(J_{01}^{\text{Fe-Fe}} + J_{02}^{\text{Fe-Fe}}) - J_{01}^{\text{Fe-Mo}} < 0\,. \tag{1}$$

The FiM stability could also not be improved by shifting the unoccupied Fe $d^{\uparrow}$ states up by ΔU and thereby increasing the intra-atomic exchange splitting [10]. We assume that the lack of stability of the FiM state is caused by too large $J_{02}^{\text{Fe-Fe}}$ and too small $J_{01}^{\text{Fe-Mo}}$ constants previously calculated. When we apply the criterion (1) to our magnetic exchange constants, the left hand side is always larger than zero, and the FiM state is stable. Nevertheless, the qualitative trend observed for increasing ΔU [10] can be confirmed by our calculations including $U_{\text{eff}}^{\text{Fe}}$, if we compare only half-metallic SFMO ($U_{\text{eff}}^{\text{Fe}} \geq 1\,\text{eV}$) – reduction of the strength of $J_{01}^{\text{Fe-Fe}}$ and $J_{02}^{\text{Fe-Fe}}$ and increasing strength of $J_{01}^{\text{Fe-Mo}}$.

(ii) In a second set of calculations, we estimated the exchange coupling within the DLM approach, which models the PM state high above the Curie temperature. In this case, the induced moments vanish. The obtained magnetic coupling constants (now all $J^{\text{Fe-Mo}}$ vanish) are also shown in Fig. 5(b). They have a similar tendency as the magnetic exchange interactions obtained from the FiM reference state, which were discussed at first.

These J_{ij} were considered to calculate the Curie temperature, using either the mean-field approximation (MFA), the random-phase approximation (RPA), or the Monte Carlo (MC) method. For the latter, the coupling constants up to a distance of 12.49 Å were used. All three methods show, in particular for half-metallic

SFMO, qualitatively a similar non-linear variation with increasing $U_{\mathrm{eff}}^{\mathrm{Fe}}$ (see Fig. 5(c)). Since the MFA usually overestimates T_{C} and RPA and MC method have similar results, we limit our discussion in the following to the results of the MC simulations.

The J_{ij} obtained in the FiM reference state within the GGA yielded a T_{C} of $\approx 604\,\mathrm{K}$, i.e., 200 K above the measured values. With increasing $U_{\mathrm{eff}}^{\mathrm{Fe}}$ but still a metallic DOS, the Curie temperature decreases linearly until $U_{\mathrm{eff}}^{\mathrm{Fe}} = 1\,\mathrm{eV}$. This corresponds with the sign change of $J_{02}^{\text{Fe-Fe}}$ and the decrease of $J_{01}^{\text{Fe-Mo}}$. For half-metallic SFMO, the theoretical critical temperatures increased slightly but stayed always 200 K below the experimental T_{C} (compare shaded area in Fig. 5(c)). The increase is observed despite the decrease of $J_{01}^{\text{Fe-Fe}}$. The stronger AFM coupling between Fe and Mo sites mediates an additional FM coupling and increases T_{C}. We obtain also from the MC simulations a FiM ground state. For the sake of completeness, the $T_{\mathrm{C}}^{\mathrm{MC}}$ for a SIC calculation is plotted as a green point and matches with the T_{C} in the limit of large $U_{\mathrm{eff}}^{\mathrm{Fe}}$ (see Fig. 5).

We note the importance of the magnetic moments at the Mo site, when considering the DLM model. The vanished Mo moments led to an increase of the magnitude of the nearest neighbor Fe–Fe coupling constants. Above $U_{\mathrm{eff}}^{\mathrm{Fe}} = 1\,\mathrm{eV}$, the first and second neighbor interactions become equal in magnitude but with different sign. Such a behavior alters the critical temperature dramatically and we observed only low ordering temperature and a ground state with vanishing averaged saturation magnetization (non-magnetic (NM), full circles in Fig. 5(c)). Although the DLM is expected to give a better description of the magnetic phase transition, its possible failure is not completely new. The induced moments of Mo might remain also above the transition temperature and the current single-site approximation of the local moments might not cover those correctly. An example of this issue was found during the investigation of the magnetic properties of Ni where only a non-local DLM approach could describe the moments sufficiently [83, 84].

In summary, the theoretical description underestimates T_{C} of half-metallic SFMO with respect to the experimental results. The value of $U_{\mathrm{eff}}^{\mathrm{Fe}} = 2\,\mathrm{eV}$ appears as a good compromise between half-metallic DOS or high T_{C}. However, there might be various reasons for the reduced value – defects like ASD or oxygen vacancies, additional electron doping or shortcomings in the description of the electronic structure. Their effect was estimated in the following sections.

C. The Curie temperature and defects

Using the CPA, we simulated at first the effect of ASD and oxygen vacancies up to 15 at. % or 10 at. %, respectively. Previous simulations or experimental measurements are only available for ASD [9, 10, 14, 86, 87]. They saw often a slight reduction of T_{C} with ASD [9, 85, 87] or an independence of ASD [14, 86] (see Fig. 6(a)).

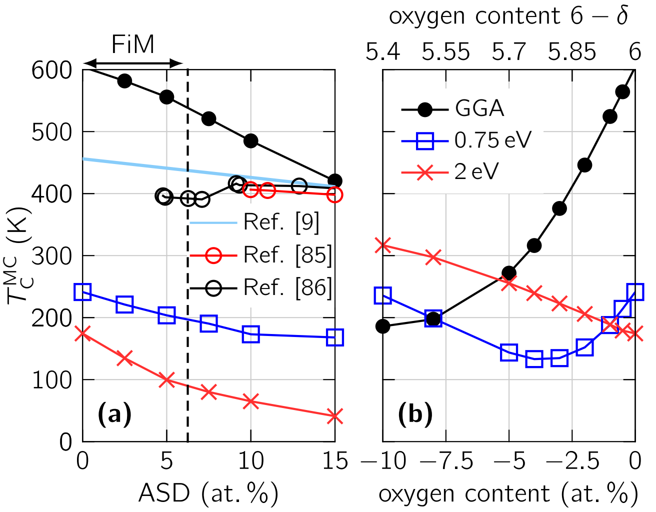

FIG. 6. Curie temperatures in dependence on the (a) ASD and (b) oxygen deficiency δ obtained with the MC method for metallic, nearly half-metallic and half-metallic SFMO (GGA, $U_{\mathrm{eff}}^{\mathrm{Fe}} = 0.75\,\mathrm{eV}$, and $U_{\mathrm{eff}}^{\mathrm{Fe}} = 2\,\mathrm{eV}$, respectively). Results of previous references are included. The FiM order is lost for more than 5 at. % ASD (marked by dashed line).

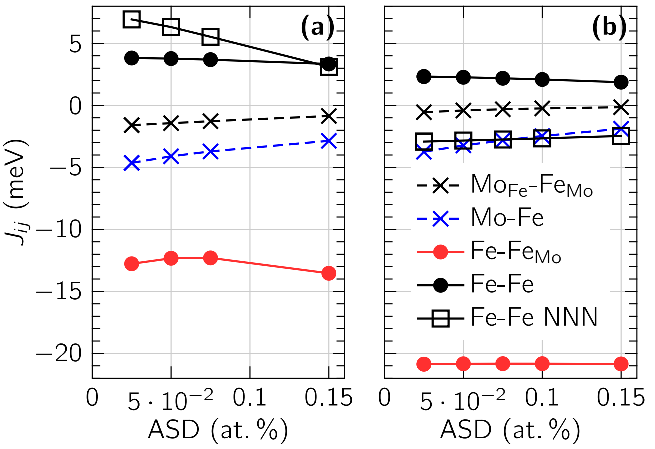

FIG. 7. Magnetic exchange interactions J_{ij} for (a) metallic and (b) half-metallic SFMO when adding ASD.

For all cases of electron correlations, T_{C} decreases with the inclusion of ASD (see Fig. 6(a)). The reduction is rather large for the GGA ($\Delta T_{\mathrm{C}} \approx 200\,\mathrm{K}$) but becomes less in the case of half-metallic SFMO ($\Delta T_{\mathrm{C}} \approx 100\,\mathrm{K}$). For the latter ($U_{\mathrm{eff}}^{\mathrm{Fe}} = 2\,\mathrm{eV}$), the slope of reduction in T_{C} decreases for larger defect concentrations around 10 at. %. This amount of ASD is a typical value found in real samples [85, 86], and the theoretical slope agrees rather well with the experimental observations or the previous Monte Carlo simulations [9]. In order to understand the observed reduction, we have again a look at the magnetic coupling constants. They vary strongly as expected for the GGA or the $U_{\mathrm{eff}}^{\mathrm{Fe}} = 2\,\mathrm{eV}$ calculation (see Fig. 7). We will mainly discuss the J_{ij} of half-metallic SFMO. By putting Fe at the Mo site ($\mathrm{Fe_{Mo}}$), a strong superexchange leads to a negative coupling constant ($\approx -21\,\mathrm{meV}$) with the original Fe sites [10] while on the other hand the $\mathrm{Mo_{Fe}}$ ions interact very weakly with the original Mo ions (not shown). The latter destabilizes the FiM ground state but at the same time the Fe-$\mathrm{Fe_{Mo}}$ magnetic interaction should be able to counteract these effects. Nevertheless, the FiM ground state collapses to an non-magnetic ordered ground state for more than 5 at. % ASD and T_C drops down (Fig. 6(a)), since the AFM Mo-Fe becomes also reduced with increasing ASD (Fig. 7(b)). We want to note that for higher amounts of antisite disorder the superexchange interactions Fe-$\mathrm{Fe_{Mo}}$ might stabilize a FiM order again with higher T_C or even dominate the magnetic coupling and form AFM order as observed in few experiments [88].

In contrast, the qualitative trend of T_C as a function of the oxygen content depends stronger on the electron correlation effects (see Fig. 6(b)). T_C becomes strongly reduced when using the GGA but it increases in half-metallic SFMO ($U_\mathrm{eff}^\mathrm{Fe} = 2\,\mathrm{eV}$). For the latter, the magnetic exchange coupling between Mo and Fe ions becomes again stronger and increases T_C by 15 K/at. %. Electron correlation close to the fringe towards half-metallicity ($U_\mathrm{eff}^\mathrm{Fe} = 0.75\,\mathrm{eV}$) showed a intermediate behavior for T_C – like for the total magnetic moment. All these observations can be understood from the effect of the oxygen vacancies to the DOS and the magnetic exchange interactions. Both quantities vary with oxygen vacancies in a similar way as observed for increasing the $U_\mathrm{eff}^\mathrm{Fe}$ parameter (cf. Figs. 2 and 5). This might be an artifact of the effective medium description used for these calculations but it worked also very well for other oxide systems [23]. Thus, the oxygen deficiency leads to a localization of Fe 3d orbitals and decreases by this the overlap integrals, which determine in a simple picture the exchange constants. We see for example that SFMO with $U_\mathrm{eff}^\mathrm{Fe} = 0.75\,\mathrm{eV}$ becomes half-metallic when adding a certain amount of oxygen vacancies (minimum at ≈ 4 at. % in Fig. 6(b)).

D. The Curie temperature and electron doping

Although we could find an estimation of the tendency of T_C as a function of the defect concentrations, the low absolute value might be attributed to various factors. We considered two possible mechanism, which might vary T_C as well, and could give another explanation for the discrepancy with the experimental T_C.

On the one hand, electron doping might result from other defects, e.g., Navarro *et al.* [89] observed for SFMO an increasing T_C by substituting Sr with La. This was related with an increase of the density of states at the Fermi energy $D(E_\mathrm{F})$. In theoretical calculations, such doping can be achieved by a shift of the Fermi energy E_F. For half-metallic SFMO, we indicate a variation by $\Delta E_\mathrm{F} = 68\,\mathrm{meV}$ in Fig. 8(a). The dashed line represents an n doping with additionally 0.15 electrons, which is related with an increase of $D(E_\mathrm{F})$ and T_C ($\approx 10\,\mathrm{K}$). This results again from a stronger magnetic coupling between the Fe and Mo ions (see Fig. S1 [71]). For a larger ΔE_F, stronger variations in the magnetic coupling constants beyond the next nearest neighbors (not shown) appeared whereby the T_C could not be increased further by electron doping.

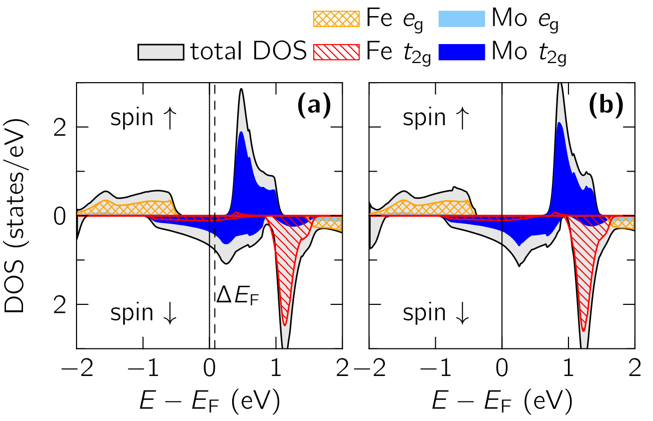

FIG. 8. LDOS of Fe and Mo around the Fermi energy calculated with $U_\mathrm{Fe} = 2\,\mathrm{eV}$ for (a) a simulated electron doping and (b) with an exemplarily $U_\mathrm{Mo} = 2\,\mathrm{eV}$. The legend is provided above the plots.

On the other hand, the electronic correlation effects were up to now only considered for the Fe d states. We found that the magnetic interaction and the Curie temperature are also very sensitive to the positions of Mo d states. The Mo d electrons of the majority spin channel are sharp and above the Fermi level, while in the minority spin channel the d electrons are located at the Fermi level forming a relatively broad band (see Fig. 8(a)). We investigated exemplarily the influence of an additional Hubbard U parameter for Mo (U_Mo) in a range of 0.5 eV to 4 eV. A small shift of spin up electrons could substantially change the Curie temperature. Since the DFT approach can not describe adequately unoccupied states, the positions of the d electrons of the majority spin channel could be not correct. We did not observe any change of $D(E_\mathrm{F})$ once we applied the U_Mo to all Mo d states. The main peak of the Mo $t_{2g}^{\downarrow}$ state retains its position above E_F but the unoccupied Mo states of the majority spin channel were shifted substantially to higher energies. This led, e.g., to $T_\mathrm{C} = 250\,\mathrm{K}$ with $U_\mathrm{Mo} = 2\,\mathrm{eV}$ (see Fig. 8(b)).

VI. X-RAY ABSORPTION AND XMCD SPECTRA

Finally, we want to return to the discussion of the valency of the Fe ions, which seems to be a mixed valency state following from experiments [28, 29, 33, 34] but is

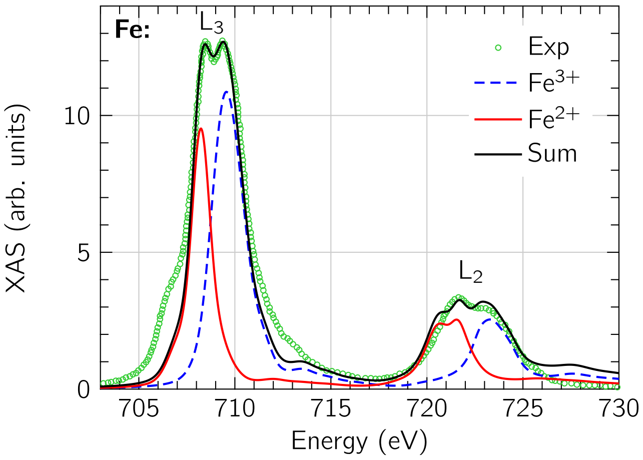

FIG. 9. (Color online) The x-ray absorption spectra (Ref. [33], open circles) at Fe $L_{2,3}$ edges as average of left and right circularly polarized light in SFMO measured at 10 K with 5 T magnetic field compared with the theoretically calculated ones for Fe^{3+} (dashed blue line) and Fe^{2+} (solid red line).

3+ in the ground state obtained by theoretical calculations [10, 11, 72]. In a complex transition metal ionic compound such as the SFMO, the x-ray absorption and XMCD spectra at the $L_{2,3}$ absorption edges can be used as fingerprints of the ground state. The experimentally measured Fe $L_{2,3}$ absorption spectrum of the SFMO single crystal (Ref. [33], average of left and right circularly polarized light) displays at both absorption edges a weak lower-energy shoulder together with a doublet structure at the white line position with almost the same magnitude (see Fig. 9). The complex fine structure of the Fe $L_{2,3}$ XAS is not compatible with a pure Fe^{3+} valency state, since we observed only one peak – similar to [36] – instead of a double peak structure. In order to provide a quantitative description of the spectral features, we took into account both Fe valencies 3+ and 2+, separately, using a primitive unit cell. The theoretically calculated Fe $L_{2,3}$ XAS agrees most closely with the experimental data by using those results in a linear combination of 60 % Fe^{3+} and 40 % Fe^{2+} (see Fig. 9), which is opposite to the calculated proportion found in Ref. [33] using the framework of the ligand-field atomic formalism.

Considering that the correct Fe valency in the SFMO ground state is 3+ as concluded in many theoretical studies, the mixed valency state might follow again from lattice defects as speculated in [36]. We investigated the influence of the two types of defects in the tetragonal supercell (see Fig. 1). For the antisite defects, we observed only the Fe^{3+} solution. This might be connected with the high defect concentration modeled within the supercell. However, a single vacancy among twelve oxygen atoms has a more realistic concentration. Self-consistent calculations in the tetragonal supercell produce the valency of the Fe ions being equal to 2.9+ and 2.4+ at the Fe1 and Fe2 sites, respectively. Therefore, the existence of the vacancy shifts the valency of the nearest Fe ion (Fe2) towards 2+. This valency change could be also observed in the CPA calculation of the DOS including oxygen vacancies (see Fig. 2).

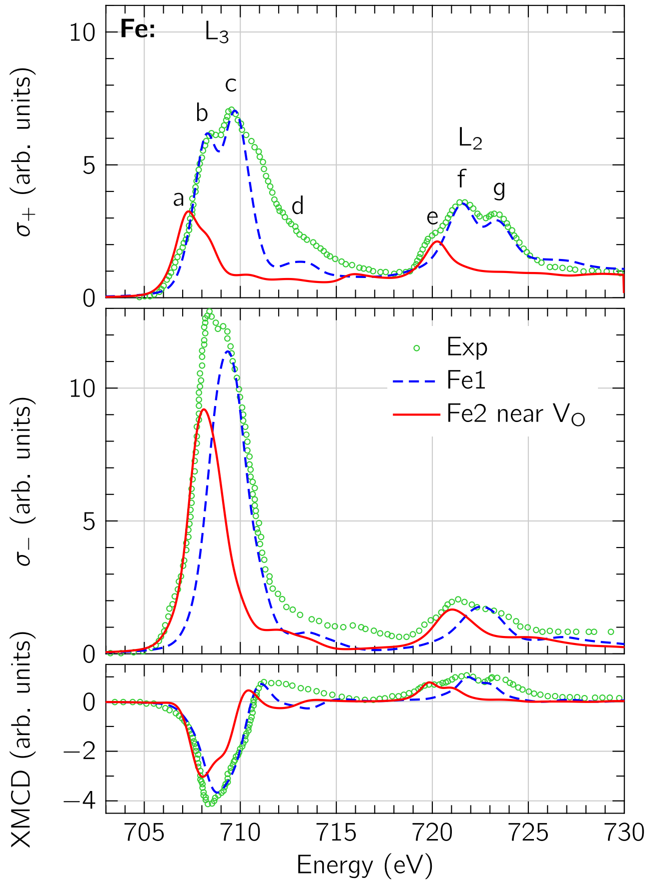

FIG. 10. (Color online) The x-ray absorption spectra (Ref. [33], open circles) at Fe $L_{2,3}$ edges in SFMO measured with left (σ^+, top panel) and right circularly polarized light (σ^-, middle panel) measured at 10 K with 5 T magnetic field and XMCD experimental spectrum (Ref. [33], lower panel) compared with the theoretically calculated spectra with an Fe ion far away (dashed blue line) and near to an oxygen vacancy (solid red line).

Indeed, the full explanation of the experimental spectra is only possible by taking into account these crystal imperfections. The Fe L_3 x-ray absorption spectrum for left circularly polarized light (σ^+) possesses four major fine structures *a*, *b*, *c* and *d* (see Fig. 10). We found that the calculations for the ideal crystal structure with the Fe^{3+} ground state solution (dashed blue line) provides the x-ray absorption intensity σ^+ only at the major peaks *b*, *c*, and *d* and do not reproduce the low energy shoulder (peak *a*) as well as the low energy peak *e* at the L_2 edge. The calculations with the Fe^{3+} solution produce only one high energy peak structure in the L_3 σ^- spectrum (middle panel). However, the experimental measurements exhibit a double-peak structure. The x-ray absorption from the Fe2 atoms with the oxygen vacancy (solid red line) contributes to the low energy peak

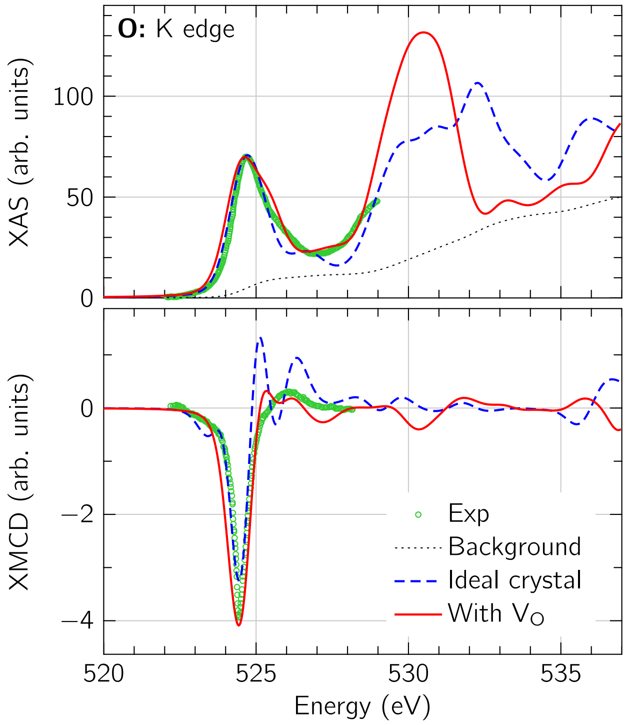

FIG. 11. (Color online) The experimental x-ray absorption spectra (Ref. [35], open circles) at O K edge (top panel) in SFMO and experimental XMCD spectra (lower panel) measured at $T = 20\,\mathrm{K}$ with $B = 1.1\,\mathrm{T}$ compared with the theoretical simulations carried out for the ideal crystal structure (solid red line) and with an oxygen vacancy (dashed blue line).

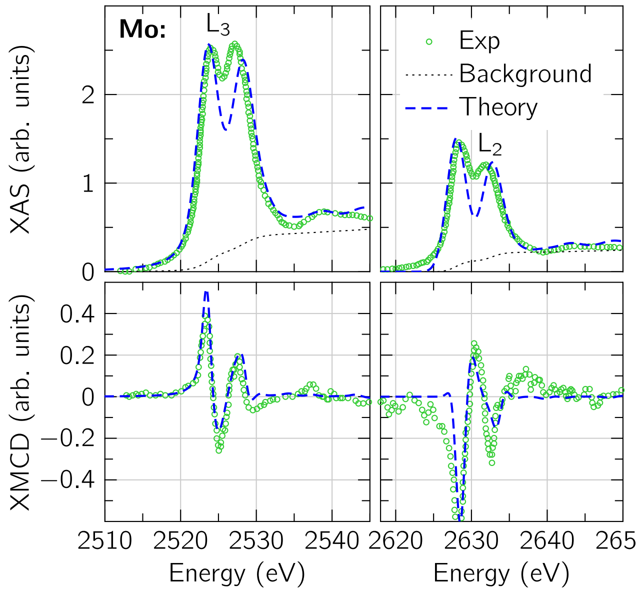

FIG. 12. (Color online) The experimental x-ray absorption spectra (Ref. [33], open circles) at Mo $L_{2,3}$ edges (top panels) in SFMO measured at 10 K with 5 T magnetic field and experimental XMCD spectra (lower panels) compared with the theoretical simulations.

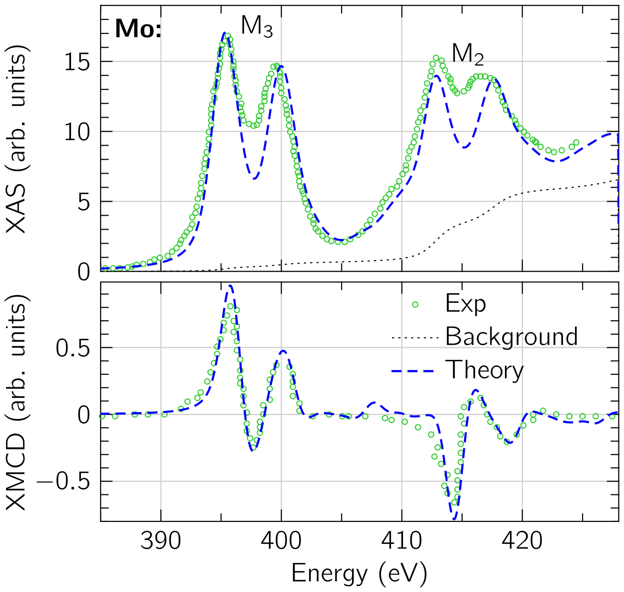

FIG. 13. (Color online) The experimental x-ray absorption spectra (Ref. [33], open circles) at Mo $M_{2,3}$ edges [90] (top panels) in SFMO and experimental XMCD spectra (lower panels) compared with the theoretical simulations.

of σ^- absorption (see Fig. 10). The relative intensity of the peaks depends on the relative concentration of the Fe1 and Fe2 ions in SFMO, in other words, the concentration of defects such as oxygen vacancies. It is similar for the oxygen K edge. The calculations including an oxygen vacancy are in better agreement with the experimental measurements in the x-ray absorption as well as in the XMCD (see Fig. 11).

In contrast, the XAS and XMCD spectra at the Mo $L_{2,3}$ and $M_{2,3}$ edges are less sensitive for the crystal defects. For both edges the agreement with the experimental measurements is quite good (see Figs. 12 and 13) [36].

VII. CONCLUSIONS

We performed an extensive study of the electronic and magnetic properties of Sr_2FeMoO_6 with the main focus on the influence of defects. In order to agree with experiments and to describe the half-metallicity of SFMO, we had to apply an U_{eff} parameter on the d states of Fe. The band gap in the upper spin channel opened already at a small value of $U_{\mathrm{eff}}^{\mathrm{Fe}} = 1\,\mathrm{eV}$. Otherwise, the system remained metallic. The best agreement with available experimental data for XAS, XMCD, T_{C}, and DOS was achieved at $U_{\mathrm{eff}}^{\mathrm{Fe}} = 2\,\mathrm{eV}$. As already discussed in previous works, the main contribution at the Fermi energy originates from the hybridized $t_{2\mathrm{g}}^{\downarrow}$ states of the Mo and Fe ions.

Only the consideration of a magnetic moment at the Mo site stabilized the ferrimagnetic ground state and yielded a reasonable T_{C}. Both kinds of lattice defects

– ASD and V_{vac} – reduced the total magnetic moment, which is in good agreement with the experimental studies. On the other hand, we found several mechanisms, which affected T_C. If the measured sample was doped with additional electrons or electron correlation effects were taken into account also for the Mo ions, T_C could be increased. Antisite disorder might have had the opposite effect and reduces T_C. The most important result is the prediction of an increasing T_C when considering oxygen vacancies as well. These vacancies seem to be also responsible for the specific magnetic dichroism spectra for the Fe $L_{2,3}$ edges observed in SFMO. We obtained only good agreement with the measured spectra including oxygen deficiency. It might be possible to estimate the amount of oxygen vacancies via fitting the experimental XAS/XMCD spectra with a particular mixture of theoretical spectra for defect-free and oxygen deficient SFMO. Finally, we can can conclude that varying defect concentrations could be in principle one reason for the observed differences in the magnetic properties of thin films or bulk samples discussed in the introduction. The appearance of defects might vary T_C in the order of $\approx 15\,\mathrm{K/at.\,\%}$.

ACKNOWLEDGMENTS

This work was funded by the *Deutsche Forschungsgemeinschaft* (DPG) within the SFB 762, “Functionality of Oxide Interfaces”.

[1] D. Serrate, J. M. De Teresa, and M. R. Ibarra, J. Phys.: Condens. Matter **19**, 23201 (2007).

[2] H. Kato, T. Okuda, Y. Okimoto, Y. Tomioka, K. Oikawa, T. Kamiyama, and Y. Tokura, Phys. Rev. B **69**, 184412 (2004).

[3] K.-I. Kobayashi, T. Kimura, H. Sawada, K. Terakura, and Y. Tokura, Nature **395**, 677 (1998).

[4] A. Venimadhav, F. Sher, J. Attfield, and M. Blamire, J. Magn. Magn. Mater. **269**, 101 (2004).

[5] W. Westerburg, D. Reisinger, and G. Jakob, Phys. Rev. B **62**, R767 (2000).

[6] D. Kumar and D. Kaur, Physica B **405**, 3259 (2010).

[7] P. Paturi, M. Metsänoja, and H. Huhtinen, Thin Solid Films **519**, 8047 (2011).

[8] M. Saloaro, H. Deniz, H. Huhtinen, H. Palonen, S. Majumdar, and P. Paturi, J. Phys.: Condens. Matter **27**, 386001 (2015).

[9] A. S. Ogale, S. B. Ogale, R. Ramesh, and T. Venkatesan, Appl. Phys. Lett. **75**, 537 (1999).

[10] I. V. Solovyev, Phys. Rev. B **65**, 144446 (2002).

[11] A. B. Muñoz García, M. Pavone, and E. A. Carter, Chem. Mater. **23**, 4525 (2011).

[12] D. Stoeffler and S. Colis, J. Phys.: Condens. Matter **17**, 6415 (2005).

[13] O. Erten, O. N. Meetei, A. Mukherjee, M. Randeria, N. Trivedi, and P. Woodward, Phys. Rev. Lett. **107**, 257201 (2011).

[14] O. Erten, O. N. Meetei, A. Mukherjee, M. Randeria, N. Trivedi, and P. Woodward, Phys. Rev. B **87**, 165105 (2013).

[15] A. M. Reyes, Y. Arredondo, and O. Navarro, J. Phys. Chem. C **120**, 4048 (2016).

[16] A. I. Liechtenstein, M. I. Katsnelson, V. P. Antropov, and V. A. Gubanov, J. Magn. Magn. Mater. **67**, 65 (1987).

[17] I. D. Hughes, M. Däne, A. Ernst, W. Hergert, M. Lüders, J. Poulter, J. B. Staunton, A. Svane, Z. Szotek, and W. M. Temmerman, Nature **446**, 650 (2007).

[18] G. Fischer, M. Däne, A. Ernst, P. Bruno, M. Lüders, Z. Szotek, W. M. Temmerman, and W. Hergert, Phys. Rev. B **80**, 014408 (2009).

[19] T.-H. Chuang, K. Zakeri, A. Ernst, L. M. Sandratskii, P. Buczek, Y. Zhang, H. J. Qin, W. Adeagbo, W. Hergert, and J. Kirschner, Phys. Rev. Lett. **109**, 207201 (2012).

[20] K. Zakeri, T.-H. Chuang, A. Ernst, L. M. Sandratskii, P. Buczek, H. J. Qin, Y. Zhang, and J. Kirschner, Nat. Nanotechnol. **8**, 853 (2013).

[21] T.-H. Chuang, K. Zakeri, A. Ernst, Y. Zhang, H. J. Qin, Y. Meng, Y.-J. Chen, and J. Kirschner, Phys. Rev. B **89**, 174404 (2014).

[22] H. J. Qin, K. Zakeri, A. Ernst, L. M. Sandratskii, P. Buczek, A. Marmodoro, T. H. Chuang, Y. Zhang, and J. Kirschner, Nat. Commun. **6**, 6126 (2015).

[23] M. Hoffmann, V. S. Borisov, S. Ostanin, I. Mertig, W. Hergert, and A. Ernst, Phys. Rev. B **92**, 094427 (2015).

[24] T. Saitoh, M. Nakatake, A. Kakizaki, H. Nakajima, O. Morimoto, S. Xu, Y. Moritomo, N. Hamada, and Y. Aiura, Phys. Rev. B **66**, 035112 (2002).

[25] J.-S. Kang, J. H. Kim, A. Sekiyama, S. Kasai, S. Suga, S. W. Han, K. H. Kim, T. Muro, Y. Saitoh, C. Hwang, C. G. Olson, B. J. Park, B. W. Lee, J. H. Shim, J. H. Park, and B. I. Min, Phys. Rev. B **66**, 113105 (2002).

[26] J. H. Kim, S. C. Wi, S. Yoon, B. J. Suh, S. W. Han, K. H. Kim, A. Sekiyama, S. Kasai, S. Suga, C. Hwang, C. G. Olson, B. J. Park, B. W. Lee, and I. Introduction, J. Korean Phys. Soc. **43**, 416 (2003).

[27] D. D. Sarma, E. V. Sampathkumaran, S. Ray, R. Nagarajan, S. Majumdar, A. Kumar, G. Nalini, and T. N. Guru Row, Solid State Commun. **114**, 465 (2000).

[28] J. Lindén, T. Yamamoto, M. Karppinen, H. Yamauchi, and T. Pietari, Appl. Phys. Lett. **76**, 2925 (2000).

[29] Cz. Kapusta, P. C. Riedi, D. Zajac, M. Sikora, J. M. De Teresa, L. Morellon, and M. R. Ibarra, J. Magn. Magn. Mater. **242-245**, 701 (2002).

[30] B. García-Landa, C. Ritter, M. R. Ibarra, J. Blasco, P. A. Algarabel, R. Mahendiran, and J. García, Solid State Commun. **110**, 435 (1999).

[31] Y. Moritomo, S. Xu, A. Machida, T. Akimoto, E. Nishibori, M. Takata, M. Sakata, and K. Ohoyama, J. Phys. Soc. Jpn. **69**, 1723 (2000).

[32] S. Ray, A. Kumar, D. D. Sarma, R. Cimino, S. Turchini, S. Zennaro, and N. Zema, Phys. Rev. Lett. **87**, 097204 (2001).

[33] M. Besse, V. Cros, A. Barthélémy, H. Jaffrès, J. Vogel, F. Petroff, A. Mirone, A. Tagliaferri, P. Bencok, P. Decorse, P. Berthet, Z. Szotek, W. M. Temmerman,

S. S. Dhesi, N. B. Brookes, A. Rogalev, and A. Fert, Europhys. Lett. **60**, 608 (2002).

[34] K. Kuepper, I. Balasz, H. Hesse, A. Winiarski, K. C. Prince, M. Matteucci, D. Wett, R. Szargan, E. Burzo, and M. Neumann, Phys. Status Solidi A **201**, 3252 (2004).

[35] T. Koide, T. Sekine, H. Miyauchi, H. Manaka, D. Asakura, A. Fujimori, K.-I. Kobayashi, Y. Tomioka, T. Kimura, and Y. Tokura, J. Phys.: Confer. Ser. **502**, 12003 (2014).

[36] V. Kanchana, G. Vaitheeswaran, M. Alouani, and A. Delin, Phys. Rev. B **75**, 220404 (2007).

[37] D. Stoeffler and C. Etz, J. Phys.: Condens. Matter **18**, 11291 (2006).

[38] E. Burzo, I. Balasz, M. Valeanu, and I. G. Pop, J. Alloys Comp. **509**, 105 (2011).

[39] Y. Moritomo, S. Xu, T. Akimoto, A. Machida, N. Hamada, K. Ohoyama, E. Nishibori, M. Takata, and M. Sakata, Phys. Rev. B **62**, 14224 (2000).

[40] S.-I. Park, H. J. Ryu, S. B. Kim, B. W. Lee, and C. S. Kim, Physica B **345**, 99 (2004).

[41] S. Nakamura and K. Oikawa, J. Phys. Soc. Jpn. **72**, 3123 (2003).

[42] A. Azad, S.-G. Eriksson, A. Khan, A. Eriksson, and M. Tseggai, J. Solid State Chem. **179**, 1303 (2006).

[43] This figure was partially prepared with VESTA [91].

[44] S. B. Kim, B. W. Lee, and C. S. Kim, J. Magn. Magn. Mater. **242-245**, 747 (2002).

[45] Y. Zhai, J. Qiao, G. Huo, and S. Han, J. Magn. Magn. Mater. **324**, 2006 (2012).

[46] HUTSEPOT is a Green's function method and developed by A. Ernst *et al.* at the Max Planck Institute of Microstructure Physics, Germany. The basic features were described in M. Lüders, A. Ernst, W. M. Temmerman, Z. Szotek, and P. J. Durham, J. Phys.: Condens. Matter **13**, 8587 (2001); M. Lüders, A. Ernst, M. Däne, Z. Szotek, A. Svane, D. Ködderitzsch, W. Hergert, B. L. Györffy, and W. M. Temmerman, Phys. Rev. B **71**, 205109 (2005).

[47] O. K. Andersen, Phys. Rev. B **12**, 3060 (1975).

[48] V. V. Nemoshkalenko, A. E. Krasovskii, V. N. Antonov, Vl. N. Antonov, U. Fleck, H. Wonn, and P. Ziesche, Phys. Status Solidi B **120**, 283 (1983).

[49] V. N. Antonov, A. Y. Perlov, A. P. Shpak, and A. N. Yaresko, J. Magn. Magn. Mater. **146**, 205 (1995).

[50] P. E. Blöchl, Phys. Rev. B **50**, 17953 (1994).

[51] G. Kresse and D. Joubert, Phys. Rev. B **59**, 1758 (1999).

[52] H. P. Xiang, Z. J. Wu, and J. Meng, Phys. Status Solidi B **242**, 1414 (2005).

[53] J. P. Perdew, K. Burke, and M. Ernzerhof, Phys. Rev. Lett. **77**, 3865 (1996).

[54] J. P. Perdew, K. Burke, and M. Ernzerhof, Phys. Rev. Lett. **78**, 1396 (1997).

[55] S. L. Dudarev, G. A. Botton, S. Y. Savrasov, C. J. Humphreys, and A. P. Sutton, Phys. Rev. B **57**, 1505 (1998).

[56] J. Staunton, B. Gyorffy, A. Pindor, G. Stocks, and H. Winter, J. Magn. Magn. Mater. **45**, 15 (1984).

[57] B. L. Gyorffy, A. J. Pindor, J. B. Staunton, G. M. Stocks, and H. Winter, J. Phys. F: Met. Phys. **15**, 1337 (1985).

[58] M. M. Otrokov, A. Ernst, S. Ostanin, G. Fischer, P. Buczek, L. M. Sandratskii, W. Hergert, I. Mertig, V. M. Kuznetsov, and E. V. Chulkov, Phys. Rev. B **83**, 155203 (2011).

[59] M. M. Otrokov, A. Ernst, V. V. Tugushev, S. Ostanin, P. Buczek, L. M. Sandratskii, G. Fischer, W. Hergert, I. Mertig, V. M. Kuznetsov, and E. V. Chulkov, Phys. Rev. B **84**, 144431 (2011).

[60] S. Tyablikov, *Methods in the Quantum Theory of Magnetism* (Springer, Berlin Heidelberg, 1995).

[61] V. N. Antonov, A. N. Yaresko, and O. Jepsen, Physical Review B **81**, 075209 (2010).

[62] J. L. Campbell and T. Parr, At. Data Nucl. Data Tables **77**, 1 (2001).

[63] P. E. Blöchl, O. Jepsen, and O. K. Andersen, Phys. Rev. B **49**, 16223 (1994).

[64] A. N. Yaresko, V. N. Antonov, and P. Fulde, Phys. Rev. B **67**, 155103 (2003).

[65] C. Meneghini, S. Ray, F. Liscio, F. Bardelli, S. Mobilio, and D. D. Sarma, Phys. Rev. Lett. **103**, 046403 (2009).

[66] A. Marmodoro, A. Ernst, S. Ostanin, and J. B. Staunton, Phys. Rev. B **87**, 125115 (2013).

[67] R. Kircheisen and J. Töpfer, J. Solid State Chem. **185**, 76 (2012).

[68] T. Yamamoto, J. Liimatainen, J. Lindén, M. Karppinen, and H. Yamauchi, J. Mater. Chem. **10**, 2342 (2000).

[69] S. Colis, D. Stoeffler, C. Mény, T. Fix, C. Leuvrey, G. Pourroy, A. Dinia, P. Panissod, and C. Meny, J. Appl. Phys. **98**, 033905 (2005).

[70] D. D. Sarma, P. Mahadevan, T. Saha-Dasgupta, S. Ray, and A. Kumar, Phys. Rev. Lett. **85**, 2549 (2000).

[71] See Supplemental Material below.

[72] Z. Szotek, W. M. Temmerman, A. Svane, L. Petit, and H. Winter, Phys. Rev. B **68**, 104411 (2003).

[73] Y. Tomioka, T. Okuda, Y. Okimoto, R. Kumai, K.-I. Kobayashi, and Y. Tokura, Phys. Rev. B **61**, 422 (2000).

[74] We note that we use here the notation $e_{\mathrm{g}}^{\uparrow}$ in accordance with other publications, although the degeneration of the d states is lifted due to the slight tetragonal distortion. The crystal field at the Fe (Mo) site (now $D_{4\mathrm{d}}$ point symmetry) splits the Fe (Mo) $3d$ ($4d$) orbitals into three singlets $A_{1\mathrm{g}}$ (d_{3z^2}), $B_{1\mathrm{g}}$ ($d_{x^2-y^2}$), and $B_{2\mathrm{g}}$ (d_{xy}) and a doublet e_{g} (d_{yz} and d_{xz}). Since the deviation from the ideal c/a ratio is only small, the states d_{xy} and d_{3z^2}, as well as the states $d_{x^2-y^2}$, d_{yz} and d_{xz}, form two groups of states, which showed an almost similar DOS. Those are considered as e_{g} and $t_{2\mathrm{g}}$.

[75] R. P. Panguluri, S. Xu, Y. Moritomo, I. V. Solovyev, and B. Nadgorny, Appl. Phys. Lett. **94**, 012501 (2009).

[76] H. Wu, Y. Ma, Y. Qian, E. Kan, R. Lu, Y. Liu, W. Tan, C. Xiao, and K. Deng, Solid State Commun. **177**, 57 (2014).

[77] Z. Fang, K. Terakura, and J. Kanamori, Phys. Rev. B **63**, 180407 (2001).

[78] T. Saha-Dasgupta and D. D. Sarma, Phys. Rev. B **64**, 064408 (2001).

[79] H.-T. Jeng and G. Y. Guo, Phys. Rev. B **67**, 094438 (2003).

[80] H. Ebert, Rep. Prog. Phys. **59**, 1665 (1996).

[81] V. N. Antonov, O. Jepsen, A. N. Yaresko, and A. P. Shpak, J. Appl. Phys. **100**, 43711 (2006).

[82] L. Balcells, J. Navarro, M. Bibes, A. Roig, B. Martínez, and J. Fontcuberta, Appl. Phys. Lett. **78**, 781 (2001).

[83] J. B. Staunton and B. L. Gyorffy, Phys. Rev. Lett. **69**, 371 (1992).

[84] J. B. Staunton, A. Marmodoro, and A. Ernst, J. Phys.: Condens. Matter **26**, 274210 (2014).

[85] Y. Moritomo, N. Shimamoto, S. Xu, A. Machida, E. Nishibori, M. Takata, M. Sakata, A. Nakamura, Y. M. Oritomo, N. S. Himamoto, X. U. Sheng, A. M. Achida,

E. N. Ishibori, and M. T. Akata, Jap. J. Appl. Phys. **40**, L672 (2001).

[86] Y. H. Huang, M. Karppinen, H. Yamauchi, and J. B. Goodenough, Phys. Rev. B **73**, 104408 (2006).

[87] D. Rubi, J. Navarro, J. Fontcuberta, M. Izquierdo, J. Avila, and M. Asensio, J. Phys. Chem. Solids **67**, 575 (2006).

[88] D. Sánchez, J. Alonso, M. García-Hernández, M. Martínez-Lope, J. Martínez, and A. Mellergård, Phys. Rev. B **65**, 104426 (2002).

[89] J. Navarro, C. Frontera, L. Balcells, B. Martínez, and J. Fontcuberta, Phys. Rev. B **64**, 092411 (2001).

[90] J. H. Song, H. J. Jang, J.-H. Park, and Y. H. Jeong, IEEE Trans. Magn. **50**, 1001104 (2014).

[91] K. Momma and F. Izumi, J. Appl. Crystallogr. **44**, 1272 (2011).

Supplemental Material

e. ***Varying magnetic coupling constants by electron doping*** In order to model electronic doping on a simple level, we varied for the calculation of the magnetic exchange parameters J_{ij} the Fermi energy, E_F, by several meV without recalculating the self-consistency loop for the density of states (DOS). The corresponding nearest and next nearest magnetic exchange parameters are plotted in Fig. S1. The antiferromagnetic (AFM) coupling between the Fe and Mo ions became again stronger. This increased also the critical temperature, T_C, by few K.

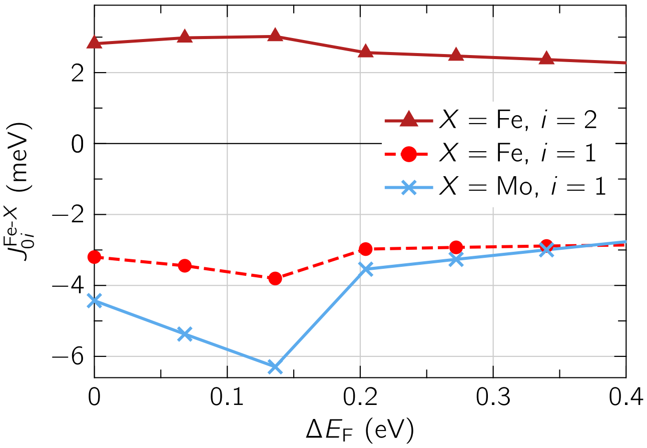

FIG. S1. Nearest and next nearest $J_{0i}^{\text{Fe-}X}$ for the coupling between Fe-Fe and Fe-Mo as a function of non-selfconsistent variation of E_F. X is either Fe or Mo and i indicated the shell number.

f. ***Electronic structure and electronic correlations in SFMO*** In order to determine an appropriate $U_\mathrm{eff}^\mathrm{Fe}$ value, we aimed to match the band gap of the majority spin channel with experimental data. The most relevant variations close to the Fermi energy happened for the Fe and Mo d states (see DOS obtained from GGA calculations in Figs. S2(a) and S3(a)). The measurement of the photoelectron spectrum (PES) by Saitoh *et al.* [S1] allowed an estimation of the position of the Fe e_g states ($\approx 1.3\,\mathrm{eV}$) assuming their comparison with a theoretical DOS calculation

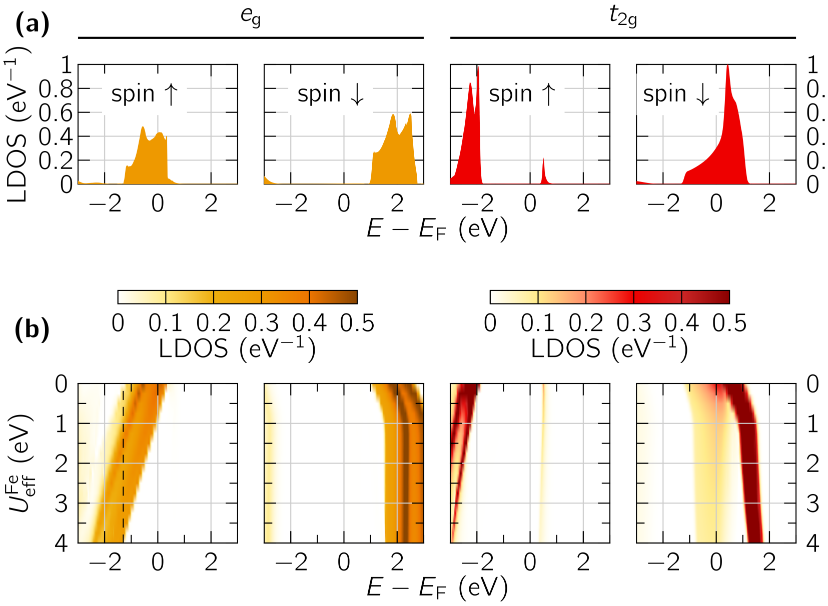

FIG. S2. Atomic and orbital resolved DOS for the Fe d states: (a) GGA calculation and (b) GGA+U. In (b) the DOS is color-coded as a contour plot. The dashed line in the left hand side panel indicates the peak position in the experimental PES [S1].

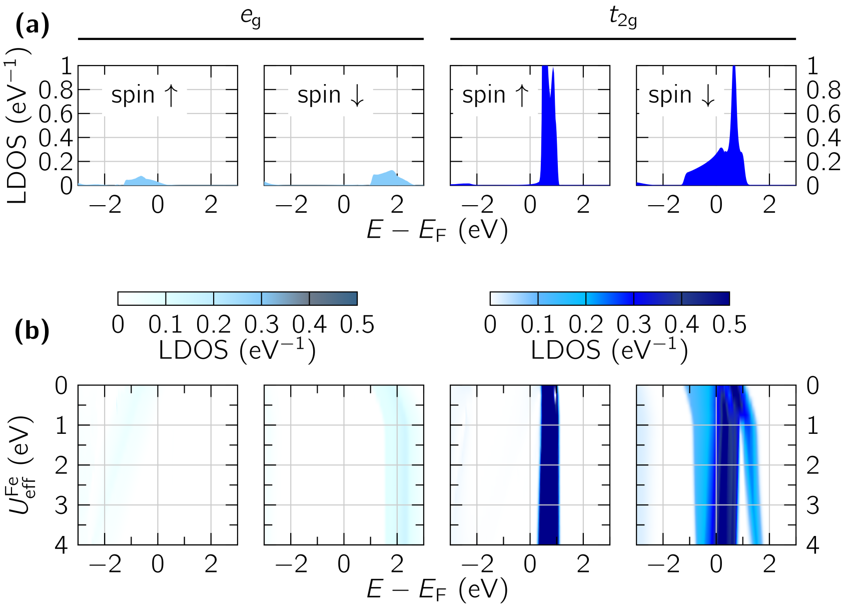

FIG. S3. Atomic and orbital resolved DOS for the Mo d states: (a) GGA calculation and (b) GGA+U. In (b) the DOS is color-coded as a contour plot.

is valid. When increasing the $U_{\mathrm{eff}}^{\mathrm{Fe}}$ parameter, the main changes at the Fermi energy appeared for the Fe e_{g} states (see Fig. S2(b), left hand side). They were pushed towards lower energies while all other states in the spin up channel did not cross E_{F} (see Figs. S2(b) and S3(b)). Thus, a band gap in the majority spin channel opened up at $U_{\mathrm{eff}}^{\mathrm{Fe}} \gtrapprox 1\,\mathrm{eV}$. In contrast, hybridizing states from the Fe and Mo $t_{2\mathrm{g}}^{\downarrow}$ states remain in the minority spin channel at E_{F}, which is why we observed half-metallic SFMO.

[S1] T. Saitoh, M. Nakatake, A. Kakizaki, H. Nakajima, O. Morimoto, S. Xu, Y. Moritomo, N. Hamada, and Y. Aiura, Phys. Rev. B **66**, 035112 (2002).